Applied Soft Computing 144 (2023) 110528

Contents lists available at ScienceDirect

Applied Soft Computing

journal homepage: www.elsevier.com/locate/asoc

Daily prediction method of dust accumulation on photovoltaic (PV) panels using echo state network with delay output

Siyuan Fan [a,*], Mingyue He [a,c], Zhenhai Zhang [b]

[a] School of Automation Engineering, Northeast Electric Power University, Jilin, 132012, China
[b] Army Engineering University of PLA, Chongqing, 400035, China
[c] Changchun Green Drive Hydrogen Technology Co. Ltd., Changchun, 130102, China

ARTICLE INFO

Article history:
Received 11 September 2022
Received in revised form 18 May 2023
Accepted 8 June 2023
Available online 14 June 2023

Keywords:
Prediction method
Dust accumulation
PV panels
Echo state network (ESN)
Pigeon inspired optimization (PIO)

ABSTRACT

Dust accumulation over time can be one of the main causes of uncertainty in the output of photovoltaic (PV) systems. In order to better understand these losses, this paper established a daily dust accumulation prediction model for PV panels based on the delay output echo state network (DESN). A pigeon-inspired optimization (PIO) algorithm with adaptive Cauchy (AC) mutation strategy was proposed, which can optimize the reservoir parameters (such as leakage rate, spectral radius, and input scaling) of DESN, shorten the solution time, and improve search speed. Based on typical meteorological and air quality data, as well as daily accumulated dust weight recorded from the experimental platform, model training and testing were carried out. According to the Pearson correlation coefficient, the relationship between the environment parameters (humidity, wind speed, wind direction, PM2.5, PM10, and rainfall) and the dust accumulation was obtained. The results show that the prediction accuracy of AC-PIO-DESN is better than other methods for meteorological and air quality data. The mean absolute percentage error (MAPE) for humidity, irradiance, PM2.5 and PM10 were 4.0743%, 4.4958%, 10.6231% and 12.8402%, respectively. In addition, the proposed daily dust prediction model has good robustness for 10-day samples, with an average relative error ranging from 0.65% to 54%. This method can provide data support for grid scheduling and PV panel cleaning strategy of PV power plants.

1. Introduction

Facing the contradiction between the consumption of traditional energy and the increasing demand for energy, the development of new energy sources is imminent [1]. Solar energy has become a major renewable energy source due to its sustainable, clean and inexhaustible characteristics [2]. Photovoltaic (PV) panels are typically installed in sparsely populated desert areas, where they are affected by wind and dust particle settling [3–5]. The accumulation of dust will reduce the light transmittance of the PV panels, thereby affecting the thermal balance and reducing the power generation efficiency and service life [6,7]. Statistically, dust accumulation can lead to a 2%–10% output loss of PV systems, reaching 25% in extreme cases [8]. A reasonable cleaning plan is required to reduce the loss of PV system due to dust accumulation, in which the dust accumulation prediction is the basis for planning [9–11]. Therefore, the accurate prediction of dust accumulation on the surface of PV panels is beneficial to improve the safety and cost-effectiveness of grid-connected PV systems.

The PV power generation system installed in natural environment is affected by many factors. The dust accumulation of PV panels is one of the main limiting factors for the output of PV power plants. Dust accumulation hinders the absorption of sunlight by PV cells, and reduces light transmittance and PV conversion efficiency. There are many studies on the effect of dust accumulation on PV performance [12,13]. Salari et al. [14] conducted numerical simulations to investigate the effect of dust deposition on the performance of PV panels. According to the research results, the electrical efficiency decreased by 26.36% as the dust accumulation increased from 0 g/m^2 to 8 g/m^2. Aslan et al. [15] conducted a 70-day outdoor experiment to analyze the impact of dust deposition on PV power generation performance. The results showed that the dust accumulation on the PV panels changed from 0 g/m^2 to 6.1 g/m^2 and the output power decreased by 21.47% after 10 weeks. In the year-long dust deposition experiment of natural and artificial deposition of Klugmann-Radziemska et al. [16], the results revealed that the efficiency of dust-covered PV panels decreased by 6%–10%. Chen et al. [17] conducted experiments to study the impact of dust

* Corresponding author.
E-mail address: fans@neepu.edu.cn (S. Fan).

https://doi.org/10.1016/j.asoc.2023.110528
1568-4946/

deposition on PV panels, and concluded that the dust density of 10 g/m^2 can reduce the maximum power of PV panels by about 34%. During the operation of PV power plants, effective prevention and cleaning are the two keys to solving the dust accumulation problem on PV panels. However, current cleaning strategies rely solely on operational experience and lack scientific evidence. Unreasonable cleaning frequency has a direct impact on the overall revenue of PV power plants. In terms of cost–benefit ratio, there is huge room for optimization.

As the outdoor exposure time of PV panels increases, the dust concentration on the PV panel surface gradually increases [18]. The change of dust accumulation on the PV panel surface is usually affected by the coupling of multiple factors, which is difficult to describe through simple mathematical model [19,20]. It seems that artificial neural network (ANN) is more suitable for this kind of complex prediction problem. Echo state network (ESN) [21] has been widely used in time series prediction [22,23] and speech recognition [24,25]. Wu et al. [26] established a model based on deep-chain echo state network (DCESN) and variational mode decomposition (VMD), which can improve the accuracy of wind power multi-step prediction. Mustaqeem et al. [27] proposed a short-term solar energy prediction model based on CNN-assisted deep echo state network (CNN-DeepESN) and principal components analysis (PCA), using 1-hour solar prediction ahead with 5-minute time intervals. Li et al. [28] proposed a growing deep ESN (GD-ESN) that can automatically determine the depth of multi-layer ESN. Furthermore, the effectiveness of the proposed method is verified in terms of benchmark datasets and practical applications. Although different forms of ESN have shown good predictive performance in the fields of wind power and PV, there is little research on the prediction of dust accumulation on PV panels. In addition to factors such as the local meteorological environment and air quality, the deposition of dust particles on PV panels is also closely related to the installation angle, orientation, height and other conditions of PV panels [29,30]. Therefore, reasonable selection of input variables and the establishment of simple and effective dust accumulation prediction model are crucial for formulating cleaning and maintenance plans for PV power plants.

Aiming at the prediction of dust accumulation on PV panel surface, an echo state network with delay output (DESN) based on the pigeon-inspired optimization (PIO) algorithm is proposed. For higher prediction accuracy, the adaptive Cauchy (AC) mutation strategy is introduced into the PIO algorithm to optimize the DESN reservoir parameters. An experimental platform for dust weight measurements of PV panels and meteorological data monitoring is established. Based on the acquired data of humidity, wind speed, wind direction, PM2.5, PM10, and rainfall, their relationship with dust accumulation is analyzed. The validity of the proposed model is verified through comparison with natural dust accumulation data.

The main contributions of this paper can be summarized as follows:

- Considering the time-delay characteristics of meteorological and air quality data, a daily prediction model of dust accumulation for PV panels based on AC-PIO-DESN is proposed.
- An AC mutation strategy is incorporated into the PIO algorithm to optimize the reservoir parameters of the DESN to improve the prediction accuracy of the model.

2. Methodology

2.1. Echo state network with delay output

ESN [31] is a type of recurrent neural network (RNN) consisting of a K-dimensional input layer, N-dimensional reservoir, and L-dimensional output layer. Let $u = u(n)$, $x = x(n)$ and $y = y(n)$ denote the external input vector, the reservoir state and the output vector, respectively. Since we consider a nonlinear system with a delayed output, the previous moment's output of the ESN is used in the reservoir state equation; thus, this network is called DESN [32]. The structure of the DESN is shown in Fig. 1.

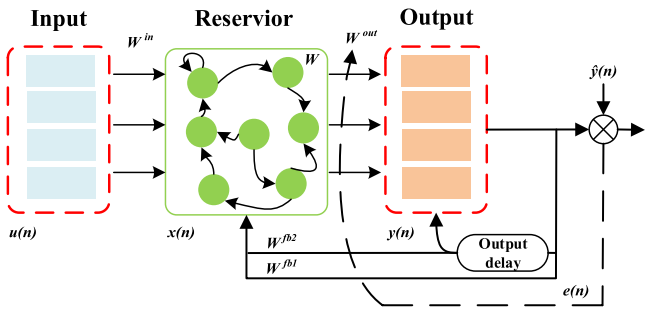

Fig. 1. The structure of the DESN.

The state update and output equation of the discrete reservoir of DESN are defined as follows:

$$x(n+1) = (1-a)x(n) + f(W^{in}u(n+1) + Wx(n) + W^{fb1}y(n) + W^{fb2}y(n-\tau)) \quad (1)$$

$$y(n) = g(W^{out}[x(n); u(n)]) - \alpha y(n-\tau) \quad (2)$$

where $a \in (0, 1]$ denotes the leaking rate, α denotes the delay factor, τ denotes the delay range, $W^{in} \in \mathbb{R}^{N\times K}$ denotes the input weight matrix, $W \in \mathbb{R}^{N\times N}$ denotes the reservoir weight matrix, $W^{fb} \in \mathbb{R}^{N\times L}$ denotes the output feedback weight matrix, and $W^{out} \in \mathbb{R}^{L\times(K+N)}$ denotes the output weight matrix.

Remark 1. When $a = 1$, $\tau = 0$, and $\alpha = 0$, DESN model is transformed into the classical ESN model. When $\tau = 0$ and $\alpha = 0$, DESN model changes to the Leaky-ESN model.

We train the output weight W^{out} of the networks to minimize the error

$$e(n) = y(n) - \hat{y}(n) \quad (3)$$

or square error

$$E(n) = \frac{1}{2}\|e(n)\|^2 \quad (4)$$

so that the predicted output $y(n)$ matches the expected output $\hat{y}(n)$. W, W^{in} and $W^{fb1,2}$ of the DESN can be determined randomly before learning and remain unchanged during learning and testing.

Let the reservoir state matrix $\overline{X} = [u(n)^T, x(n)^T]^T$, the desired output matrix $Y^{teach} = [y(1), y(2), \ldots, y(P)]$, and the computed output weight matrix W^{out} satisfies:

$$\overline{X}W^{out} = Y^{teach} \quad (5)$$

The output weight matrix W^{out} can be solved using linear regression. Various learning algorithms (the Pseudo-inverse method, Wiener–Hopf method, Kalman filter, etc.) can be used to obtain the weights of the DESN. In this paper, the Pseudo-inverse method is used to solve the output weights; the calculation equation is:

$$W^{out} = \overline{X}^{\dagger}Y^{teach} \quad (6)$$

2.2. Parameter optimization method

In practical applications of the DESN prediction model, we need to optimize the reservoir parameters to minimize the training error and obtain a high prediction accuracy. Eq. (1) can be modified as follows to obtain spectral radius of matrix W:

$$\begin{aligned}\frac{1}{\gamma}x(n+1) =&(1-a)\frac{1}{\gamma}x(n)+f(W^{in}u(n+1)+(\gamma W)\frac{1}{\gamma}x(n)\\ &+W^{fb1}y(n)+W^{fb2}y(n-\tau))\end{aligned} \tag{7}$$

where γ denotes the spectral radius of the reservoir, and $\gamma > 0$.

Without loss of generality, $\frac{1}{\gamma}x(\cdot)$ is always written as $x(\cdot)$. In order to normalize the weight matrices W^{in}, W^{fb1} and W^{fb2}, we modify the Eq. (8) as follows:

$$\begin{aligned}x(n+1) =&(1-a)x(n)+f(s^{in}W^{in}u(n+1)+(\gamma W)x(n)\\ &+s^{fb1}W^{fb1}y(n)+s^{fb2}W^{fb2}y(n-\tau))\end{aligned} \tag{8}$$

where s^{in} denotes the scalings of the input, and s^{fb1} and s^{fb2} are the scalings of the output feedback and the delay output feedback.

2.3. AC-PIO algorithm

The PIO algorithm [33] is a novel intelligence optimization algorithm for solving global optimization problems. It simulates the homing behavior of pigeons that use the earth's magnetic field and landmarks [34]. When a pigeon is far away from its destination, it uses the earth's magnetic field to identify the flight direction. When a pigeon is close to its destination, it uses landmarks for navigation.

(1) Map and compass operator

In the map and compass operator, the rules are defined using the position X_i and the velocity V_i of i pigeon, which are updated in a D-dimensional search space in each iteration. The new position X_i and velocity V_i of i pigeon in the th iteration can be calculated as follows:

$$V_i(n) = V_i(n-1) * e^{-Rn} + rand * (X_{gbest} - X_i(n-1)) \tag{9}$$

$$X_i(n) = X_i(n-1) + V_i(n) \tag{10}$$

where R denotes map and compass factor, $rand$ denotes a random number, and X_{gbest} denotes the global best position.

(2) Landmark operator

In landmark operator, N_p is used to record the half number of pigeons in each generation, and $X_c(n)$ is the center position of all pigeons in generation n. If each pigeon can fly a direct distance to a destination, the position updating rule for pigeon ith iteration is described as follows:

$$N_p(n) = \frac{N_p(n-1)}{2} \tag{11}$$

$$X_c(n) = \frac{\sum X_i(n) * fitness(X_i(n))}{N_p * \sum fitness(X_i(n))} \tag{12}$$

$$X_i(n) = X_i(n-1) + rand * (X_c(n) - X_i(n-1)) \tag{13}$$

where $fitness(x)$ denotes the quality of the individual pigeon. For the minimum optimization problem, $fitness(X_i(n)) = 1/(f_{min}(X_i(n)) + \varepsilon)$; otherwise, $fitness(X_i(n)) = f_{max}(X_i(n))$. The adaptive weight coefficient ω is defined as follows:

$$\omega = \omega_{max} - \frac{(\omega_{max} - \omega_{min})n}{N_{iter}} \tag{14}$$

where n denotes the current number of iterations, and N_{iter} denotes the predefined maximum number of iterations.

The Cauchy density function can be defined as follows:

$$f(x; x_0, \gamma) = \frac{1}{\pi}\left[\frac{\gamma}{\gamma^2 + (x - x_0)^2}\right], x \in (-\infty, +\infty) \tag{15}$$

The corresponding distribution function is described as follows:

$$F(x; x_0, \gamma) = \frac{1}{\pi}\arctan(\frac{x - x_0}{\gamma}) + \frac{1}{2} \tag{16}$$

When $x_0 = 0$, $\gamma = 1$ is the standard Cauchy distribution, which is defined as follows:

$$f(x; 0, 1) = \frac{1}{\pi(1 + x^2)} \tag{17}$$

The AC mutation strategy is used in the PIO algorithm, and the position update is defined as follows:

$$X_i(n) = X_i(n-1) + C_1\omega(X_c(n) - X_i(n-1)) \tag{18}$$

where C_1 denotes the random number of Cauchy distributions.

2.4. Regulate DESN with AC-PIO

AC-PIO algorithm is used to optimize the reservoir parameters (i.e. leaking rate a, spectral radius γ, input scalings s^{in}) of DESN by minimizing the RMSE. The parameters are treated as three particles, which constantly update their positions and velocities, and their fitness values are calculated by the objective function to achieve the global optimum.

In this study, the objective function is the root mean square error (RMSE)

$$RMSE = \sqrt{\frac{1}{N}\sum_{n=1}^{N}(y(n) - \hat{y}(n))^2} \tag{19}$$

where N denotes the number samples.

An algorithmic implementation for optimization process is provided in **Algorithm 1**.

Algorithm 1
AC-PIO-DESN algorithm

Input: number of pigeons n, number of iterations for optimization N_{iter}, the map and compass factor R;
Output: trained AC-PIO-DESN;
Step 1: initialize N_{iter} and n pigeons positions at random $\in [0.00001, 1]$;
Step 2: compute the fitness of each pigeon;
Step 3: update velocity V_i and position X_i according to Eqs. (9) and (10);
Step 4: update position X_i according to Eq. (18);
Step 5: update a, γ, and s^{in};
Step 6: obtain optimal $RMSE$.

2.5. Dust prediction model

The degree of dust accumulation is affected by the exposure time of the PV panels in a natural environment. Researchers have used meteorological and air quality data to establish prediction models for dust accumulation of PV panels. The dust accumulation prediction problem is transformed into a prediction of the environmental parameters. In [35], a simple model for the time-series prediction of dust accumulation was proposed. This model evaluated the dust accumulation over time using the PM2.5 and PM10 concentrations in the atmospheric environment and the installation angle of the PV panels. The dust concentration during period t can be expressed as:

$$m = \int (v_{PM10}C_{PM10} + v_{PM2.5}C_{PM2.5})t\cos\theta dt \tag{20}$$

where v_{PM10}, $v_{PM2.5}$ denote the deposition rates of airborne particles whose diameters are less than or equal to 10 μm and 2.5 μm,

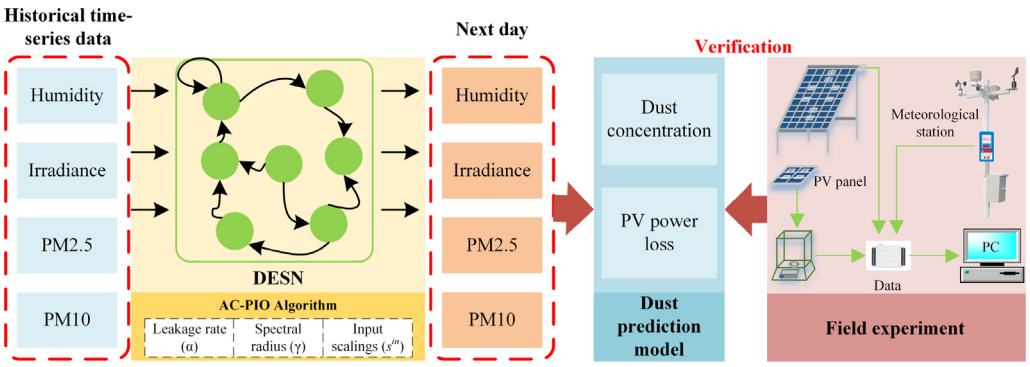

Fig. 2. Schematic diagram of the daily dust prediction model establishment and experimental verification.

respectively. C_{PM10}, $C_{PM2.5}$ denote the corresponding concentrations of particulate matter in the air, respectively. t denotes the time step, and θ denotes the installation angle of the PV panels.

Similarly, Paudyal et al. [36] studied the effect of dust accumulation on the PV panels. A regression equation describing dust concentration, environmental parameters and PV power loss is established, which can be described as:

$$\eta_{dust} = A + \beta_1 X_1 + \beta_2 X_2 + \beta_3 X_3 + \beta_4 X_4 + \beta_5 X_5 + \beta_6 X_6 \tag{21}$$

where A denotes the regression coefficient, X_1 denotes the temperature of PV panels, X_2 denotes the dust concentration, X_3 denotes the humidity, X_4 denotes the irradiance, X_5 denotes the rainfall, and X_6 denotes the ambient temperature.

According to Eqs. (20) and (21), the dust weight and the power loss of PV panels in a period of time can be obtained. Since the above model uses historical time-series data, delays occur, which can be addressed by the DESN. Hence, the dust accumulation prediction model based on AC-PIO-DESN is established.

3. Case description

The schematic diagram of the establishment and experimental verification of the daily dust prediction model is shown in Fig. 2. The inputs include meteorological and air quality data, such as humidity, irradiance, PM2.5 and PM10. First, daily average historical time-series data are used to train the DESN model. Second, the AC-PIO algorithm is used to optimize the leakage rate, spectral radius, and input scaling. Then, the output results of the DESN model are substituted into the dust prediction model to obtain the dust concentration and PV power loss. Finally, the accuracy of the daily dust prediction model is verified through field tests.

3.1. The experimental process

Two installation angles (0° and 45°) are evaluated to verify the effect of the PV panel inclination on the dust deposition. Two comparative experiments are conducted in the same environment to ensure the same conditions. Eight glass sheets are evenly laid on the surface of the PV panels at two angles to measure the dust weight. Panels 1#, 3#, 5#, and 7# are used to measure the dust weight daily, and panels 2#, 4#, 6#, and 8# are used to measure the accumulated dust weight. The daily measurement interval is 24 h, and the cumulative time is continuous. The experimental platform for the dust weight measurements on the PV panels surface and meteorological data monitoring is shown in Fig. 3.

A PC6 meteorological station is used to record the wind speed, wind direction, temperature, and humidity, and other environmental data. The air quality data and rainfall amount are obtained from the local environmental monitoring institution. A Sartorius BT 125D is used to measure the weight of the glass sheets. The experimental equipment is shown in Fig. 4. The characteristics of the PV panel are listed in Table 1.

Table 1
The characteristics of the PV panel.

Characteristics	Value
Cell type	Mono-crystalline silicon
Maximum power (W)	260
Voltage in open circuit (V)	37.7
Short circuit current (A)	8.95
Voltage at maximum power (V)	30.3
Current at maximum power (A)	8.58
Dimension of the module	1640 mm × 990 mm × 35 mm
Test conditions	1000 W/m^2, AM 1.5, T = 25 °C

Glass sheets with a size of 150 mm×20 mm×3 mm consisting of the same material are placed on the PV panel. The weight ΔM_i of the dust is calculated as follows:

$$\Delta M_i = \frac{M_{fi} - M_{qi}}{N_{gs}} \tag{22}$$

where M_{qi} and M_{fi} denote the weight of glass sheets before and after measurements, respectively. $N_{gs} = 4$ denotes the number of glass sheets.

The experimental steps for obtaining the accumulated dust weight are as follows:

Step 1. Two PV panels are placed at an angle of 0° and 45° with the ground, respectively, and the glass sheets with the same size are evenly distributed on the surface of the PV panel. They are attached with two clips.

Step 2. The 1#-8# glass sheets are removed at 4:00 PM every day, and Sartorius BT 125D electronic balance is used to obtain the weight M_{fi}.

Step 3. Panels 1#, 3#, 5#, and 7# are cleaned, weighed to obtain the weight M_{qi}, and re-attached to the PV panel.

Step 4. Panels 2#, 4#, 6#, and 8# are attached to the PV panel without any treatment so that the dust naturally settles and evenly adheres to the surface of the PV panel.

Step 5. Powder-free latex gloves are worn by the personnel during the experiment to prevent the loss of dust particles, and the glass sheets are handled using experimental tweezers.

Step 6. Eq. (22) is used to determine the weight differences of panels 1#, 3#, 5#, and 7# to obtain the daily accumulated dust weight.

Step 7. The above steps are repeated to record the daily and accumulated dust weight of the glass sheets.

3.2. Performance indices

The data recorded by the monitoring system are used to train and verify the model. The relative error, root mean square error

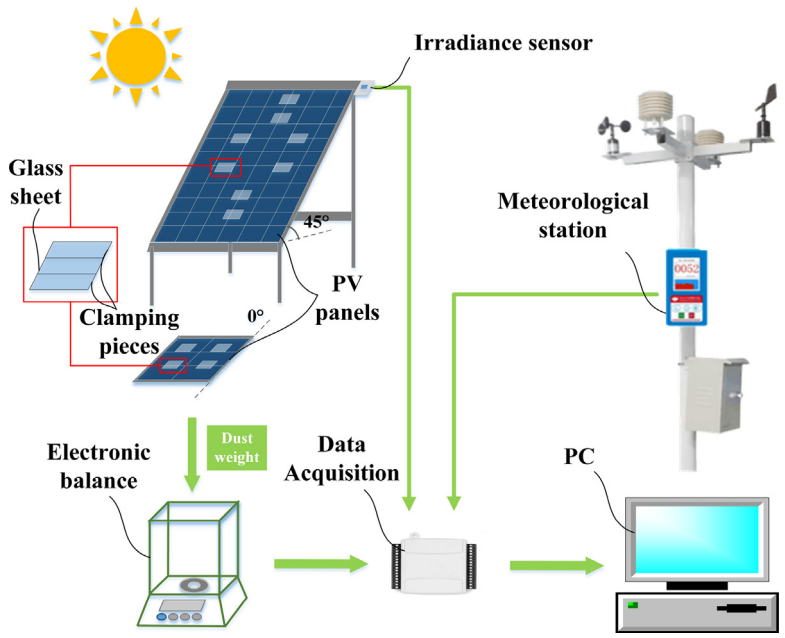

Fig. 3. The experimental platform for dust weight measurement and meteorological data monitoring.

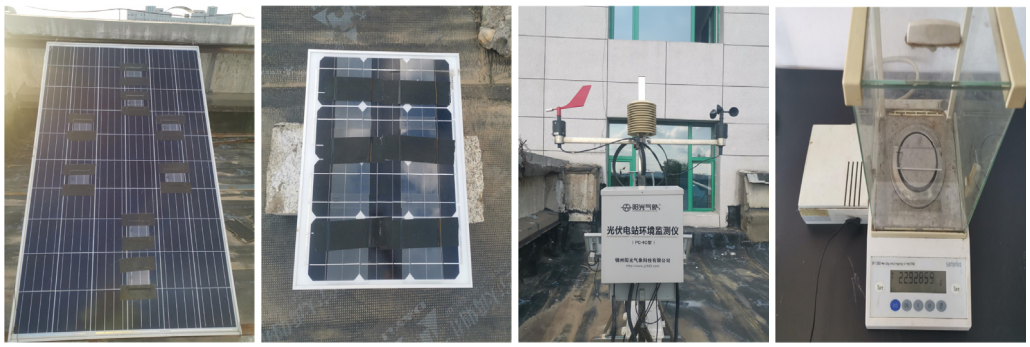

(a) 45° (b) 0° (c) PC6 meteorological station (d) Sartorius BT 125D

Fig. 4. Experimental equipment.

(NRMSE), and mean absolute percentage error (MAPE) are used to evaluate the performance. They are defined as follows:

$$e = \frac{|y_n - \hat{y}_n|}{y_n} \tag{23}$$

$$NRMSE = \sqrt{\sum_{n=1}^{N} \frac{(y(n) - \hat{y}(n))^2}{N\sigma^2}} \tag{24}$$

$$MAPE = \frac{1}{N} \sum_{n=1}^{N} \left| \frac{\hat{y}(n) - y(n)}{y(n)} \right| \times 100\% \tag{25}$$

4. Results

4.1. Installation angle

The data monitoring system is deployed on the roof of a university building in Jilin, China. The dust accumulation is affected by the wind speed, wind direction, and particle concentration. The effects of different installation angles on the daily and accumulated dust weights on the PV panels are shown in Fig. 5.

The weight of the daily dust accumulation is higher for the PV panels with an angle of 0° than 45°. The difference in the accumulated weight between the panels with the two angles is small at the beginning of dust accumulation. In an area with little rainfall, more dust is accumulated on a panel with an angle of 0° than 45°. If it rains, the dust weight will decrease, or all the dust will be washed off. The smaller the installation angle, the more dust is accumulated. Part of the dust is blown off by the wind, especially if the wind is blowing in a horizontal direction and the installation angle is small. Dust is affected by the rain. PV panels with a larger installation angle are more likely to be washed clean, and PV panels with a smaller installation angle are more likely to have rain spots.

4.2. Correlation analysis

Since the dust weights are similar at different angles, the Pearson correlation coefficient [32] is used to analyze the relationship between dust accumulation and environmental factors.

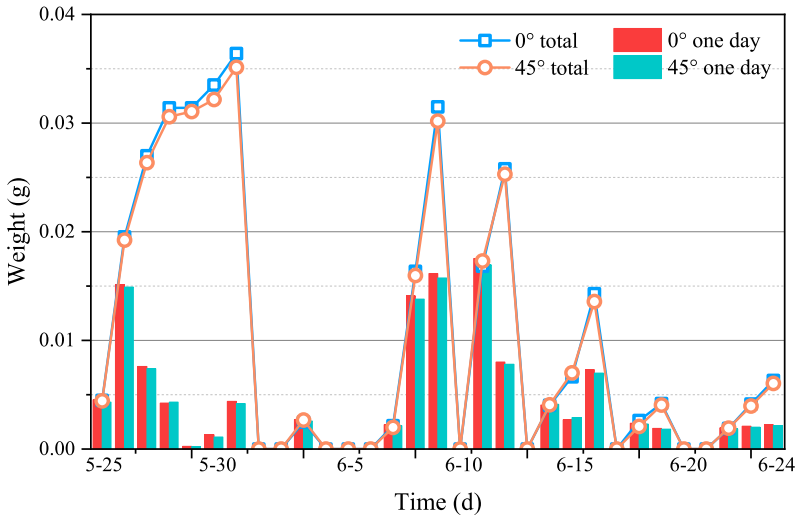

Fig. 5. The daily and accumulated dust weights on PV panels with different installation angles.

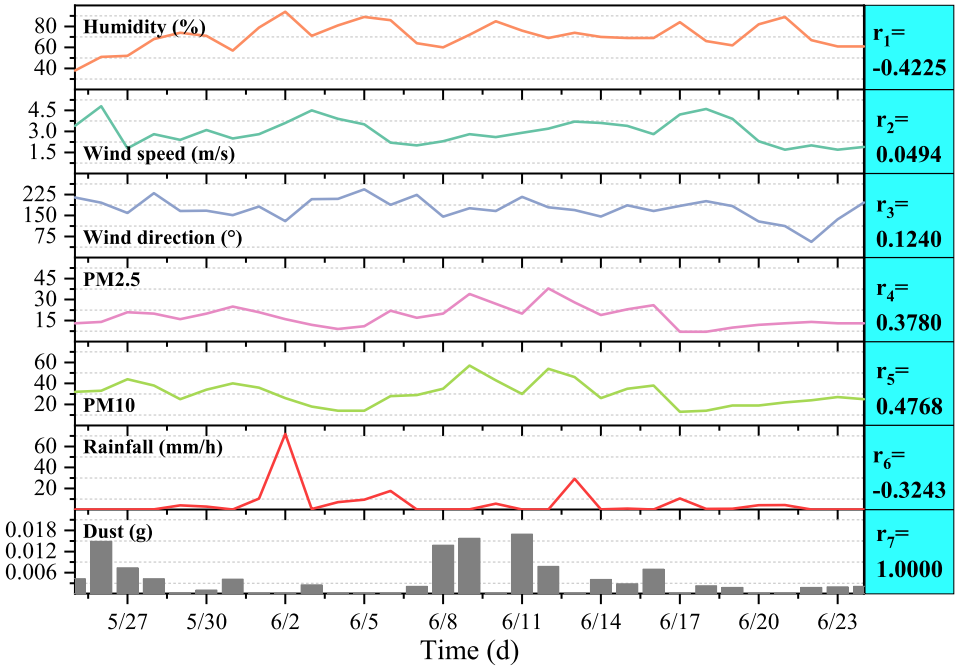

Fig. 6. The results of the correlation analysis between the dust accumulation and environmental factors.

The Pearson correlation coefficient is defined as follows:

$$r = \frac{\sum_{j=1}^{t}(x_j - \bar{x})(p_j - \bar{p})}{\sqrt{\sum_{j=1}^{t}(x_j - \bar{x})^2 \cdot \sum_{j=1}^{t}(p_j - \bar{p})^2}} \tag{26}$$

where x_j and p_j are the jth sample point for x and p, and $\bar{x}$ and $\bar{p}$ are the mean values of t samples for x and p, respectively.

It is observed in Fig. 6 that the PM is the dominant factor affecting dust deposition. PM10 has the largest correlation coefficient r (0.48), and the coefficient of PM2.5 is 0.38. This result indicates that larger dust particles are more susceptible to deposition. The wind speed and wind direction affect the dust deposition on the PV panels, but their correlation coefficients are small (0.05 and 0.12, respectively). The air humidity and rainfall are negatively correlated with the dust weight, and the rainfall has a higher correlation coefficient. The experimental results show that the dust is completely removed from the PV panel when the rainfall amount exceeds 40 mm/h.

4.3. Optimization results

The data obtained from the monitoring system are used for training and verification of the proposed model. Ambient temperature is selected to analyze the optimization performance of the proposed algorithm. In order to prove the effectiveness of ACPIO, particle swarm optimization (PSO) algorithm [37], genetic algorithm (GA) [38] and original PIO algorithm [33] are used to forecast with the same dataset. The training sample size is 1500, the initial sample size is 50, the predicted sample size is 100, and the reservoir size of the DESN is 80. The number of pigeons is 50, the particle dimension is 3, R is 0.3, and the maximum iteration step number is 50. To avoid the effects of

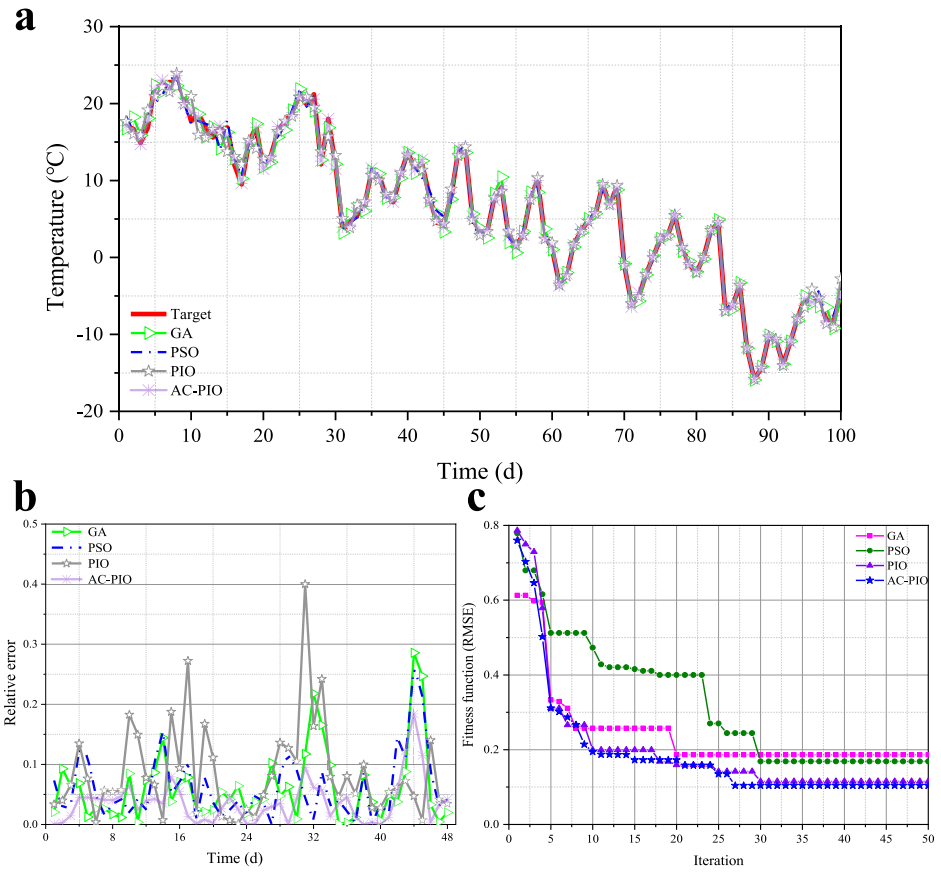

Fig. 7. Prediction results and iterative curves of four optimization methods.

Table 2
Comparison results of AC-PIO algorithm with different *R*.

Cases	Map and compass factors (*R*)	RMSE	MAPE (%)	Relative error (*e*)
1	0.1	0.86539	11.70003	0.08369
2	0.3	0.68628	6.48814	0.04591
3	0.5	0.78053	11.20039	0.09033
4	0.7	1.02079	12.72392	0.09828
5	0.9	1.21511	15.42400	0.12235

random initialization of parameters, each experiment is repeated 5 times and the average is chosen as the result. The validation performances of four methods are shown in Fig. 7.

It can be seen that the prediction results of AC-PIO algorithm are essentially coincident with the target, and its prediction ability is much higher than other models. Fig. 7(b) exhibits the relative errors of every algorithm within 48 days, and it can be clearly learned that the average relative error of AC-PIO is the smallest, reaching 0.03735. Fig. 7(c) indicates that AC-PIO achieves the smallest RMSE within 27th iterations.

To further validate the performance of the proposed method, the AC-PIO given different map and compass factors *R* are implemented for the comparison. When the reservoir size of DESN is 80, the comparison results of AC-PIO algorithm with different map and compass factors are listed in Table 2.

Table 2 presents the prediction performance of ambient temperatures with different map and compass factors. Within the five cases, $R = 0.3$ shows the best performance with 0.68628, 6.48814%, and 0.04591 of RMSE, MAPE, and relative error, respectively. In this study, AC strategy is introduced to improve the diversity of pigeon population. In fact, there is no regularity in the selection of parameters in PIO algorithm, and trial and error method is usually used to obtain the appropriate initial value. In the future, we will analyze the relationship between the parameters selection of AC-PIO and the prediction accuracy to achieve higher performance.

4.4. Environmental prediction results

A prediction model with excellent performance is crucial to provide accurate environmental information. Irrelevant variables are eliminated, and those with the greatest influence on dust accumulation are retained. In order to further evaluate the performance of AC-PIO-DESN, three other ESN models are selected for performance comparisons, including ESN [31], Leaky-ESN [39], and DESN [32]. Similarly, each experiment is repeated 5 times, and the average value is chosen as the result. The same training and test samples are used, and the RMSE, NRMSE, and MAPE are used as performance indicators. The prediction results of the different methods are listed in Table 3.

The results show that the AC-PIO-DESN has higher utilization of the output information and higher prediction accuracy than the other three methods due to the delay output and parameters optimization. Leaky-ESN and DESN models consider the delay characteristics of the reservoir, and the predicted results are generally higher than that of the ESN. The AC-PIO-DESN has the smallest NRMSE. Since it uses the PIO to optimize the DESN parameters, better results are obtained for predicting the amount of PM2.5 and PM10, with NRMSE values of 0.11686 and 0.23564, respectively.

The predicted humidity, irradiance, PM2.5, and PM10 for the four methods are shown in Fig. 8.

A small deviation is observed between the prediction results of the four methods and the experimental. The prediction results

Table 3
Comparison of the prediction results for different methods.

Cases	Methods	Optimized parameters			Reservoir size (N)	RMSE	Training NRMSE	Testing NRMSE
		a	γ	s^{in}				
Humidity	ESN [31]	–	0.52768	0.18545	80	5.95515	0.29915	0.33039
	Leaky-ESN [39]	0.65251	0.66864	6.51453	80	6.51453	0.32725	0.36142
	DESN [32]	0.44251	0.59410	0.28335	80	5.17671	0.26005	0.28720
	AC-PIO-DESN	0.30137	0.61341	0.13021	80	3.63109	0.18241	0.20145
Irradiance	ESN [31]	–	0.56865	0.08572	80	13.60189	0.19774	0.23071
	Leaky-ESN [39]	0.33362	0.42511	0.02479	80	11.32143	0.15224	0.19203
	DESN [32]	0.50387	0.47196	0.09594	80	5.08796	0.06876	0.08630
	AC-PIO-DESN	0.67627	0.27485	0.09976	80	4.55919	0.05478	0.07733
PM2.5	ESN [31]	–	0.72545	0.13179	80	4.51470	0.23365	0.25598
	Leaky-ESN [39]	0.96124	0.23731	0.19519	80	4.22026	0.19656	0.23928
	DESN [32]	0.42630	0.40599	0.15788	80	2.63813	0.12571	0.14958
	AC-PIO-DESN	0.12866	0.02843	0.14877	80	2.06109	0.09338	0.11686
PM10	ESN [31]	–	0.38199	0.97813	80	10.29279	0.35243	0.37188
	Leaky-ESN [39]	0.59787	0.33647	0.10935	80	8.16623	0.26115	0.29505
	DESN [32]	0.42714	0.21893	0.07516	80	7.15628	0.22451	0.25856
	AC-PIO-DESN	0.11322	0.12469	0.07119	80	6.52209	0.22684	0.23564

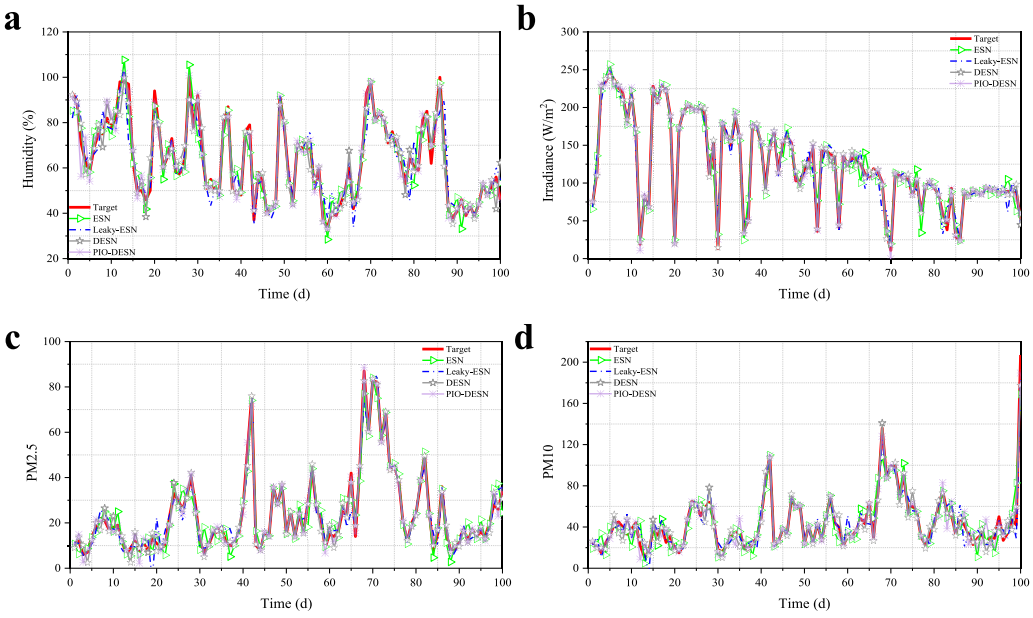

Fig. 8. Prediction results of the four methods.

of the humidity are the most accurate and the data consistency is the highest. The prediction results are the worst for PM10, although the trends are similar, but the accuracy is low. The AC-PIO-DESN has the smallest deviation from the experimental data for the meteorological and air quality data. The box plots of the relative errors are shown in Fig. 9.

The AC-PIO-DESN method has the lowest average error and the fewest outliers, making it the most suitable prediction method for practical applications. The comparison of the MAPEs of the four methods is shown in Fig. 10.

The results indicate that the humidity is stable and has the highest prediction accuracy. The MAPE of AC-PIO-DESN is 4.0743%, which is 1.80 times lower than that of the ESN, 1.64 times lower than that of the Leaky-ESN, and 1.44 times lower than that of the DESN. However, the prediction accuracy of ESN, Leaky-ESN, and DESN for PM10 and PM2.5 is relatively low, indicating that the particle concentration in the air is unstable. The average MAPE of four environmental parameters is about 8.0084%. The AC-PIO-DESN has the highest prediction accuracy, with an MAPE of 10.6231% and 12.8402% for PM2.5 and PM10, respectively. The AC-PIO-DESN provides the highest accuracy for the four parameters, with a MAPE that is nearly 2 times lower than that of the ESN.

4.5. Dust prediction results

For the verification of the accuracy of the proposed dust prediction method, the PV panel installed at an angle of 45° is used. The 24-hour average value of environmental parameters is taken as the daily value. The input time scale of the daily dust prediction model is day. The model inputs are meteorological and air quality data, including temperature, humidity, irradiance, PM2.5, and PM10, and the model output is dust concentration. The measurement experiment of dust weight is conducted without rain. The training sample size is 1500, and the initial sample size is 50. Based on the predicted results for PM2.5 and PM10, Eq. (20) is used to obtain the dust concentration, and Eq. (21) is used to obtain the PV power loss. The source of dust is presumed

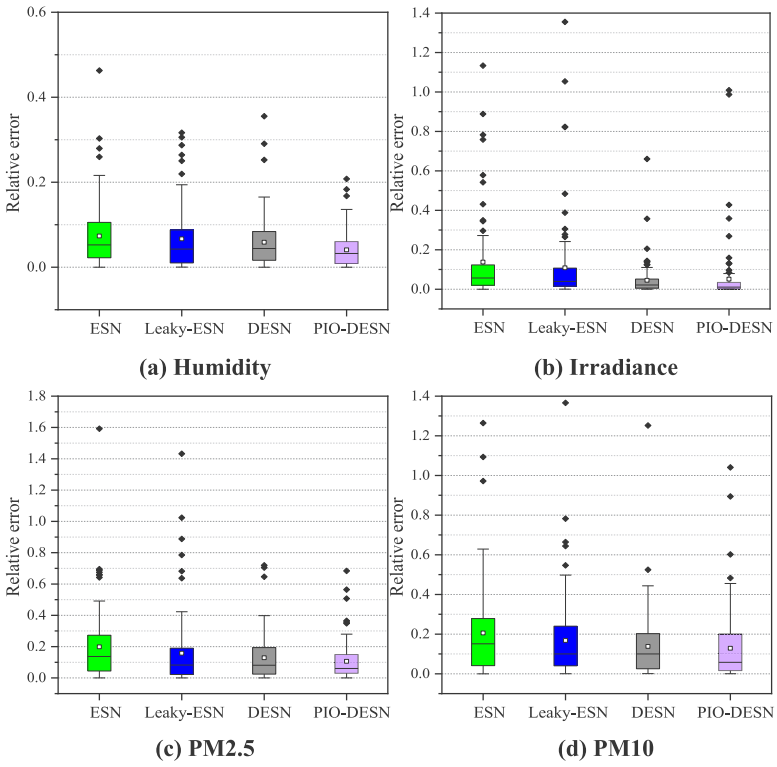

Fig. 9. Relative errors of the four methods.

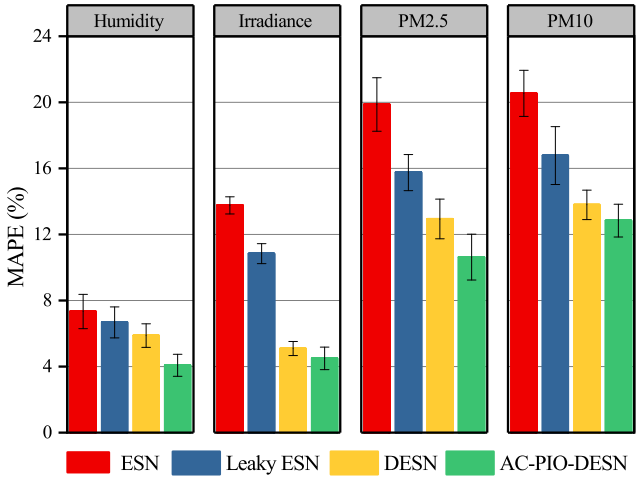

Fig. 10. The comparison of the MAPEs of the four methods.

to be particulate matter in the air. Similar to [35], deposition velocity is used instead of the deposition rate. v_{PM10} and $v_{PM2.5}$ are 0.4 cm/s and 0.09 cm/s, respectively. The comparison results between the actual and predicted values are shown in Fig. 11.

The results reveal that the overall prediction accuracy of the daily dust prediction model is relatively high, with an average relative error of 20.25% and a wide fluctuation range from 0.65% to 54%. However, dust accumulation on the surface of PV panels is a complex process, which is affected by many external factors. As for Coello's model [39], the neglect of the effect of wind may be an important factor affecting the prediction accuracy. According to the prediction results, the power loss of PV system due to dust accumulation can be obtained from 15.80% to 19.69%, which indicates that dust accumulation has a serious impact on the PV output performance. Moreover, unreasonable cleaning frequency will affect the overall income of the PV power station. Therefore, accurate prediction of dust concentration and data support for formulation of PV system cleaning and maintenance strategies are of great significance.

5. Conclusions

This paper proposed a novel dust deposition prediction method for PV panels based on AC-PIO-DESN. An experimental platform for dust weight measurements of PV panels was developed to verify the effectiveness of the proposed method. The correlation between meteorological and air quality data and the dust accumulation on PV panels with 0° and 45° installation angles were analyzed. Humidity, irradiance, PM2.5, and PM10 were used to predict the dust concentration and PV power loss.

The main conclusions are summarized as follows:

1. PM10 and PM2.5 were the main factors affecting dust deposition, with correlation coefficients of 0.48 and 0.38, respectively. When the rainfall exceeded 40 mm/h, the dust was completely removed from the PV panels.
2. The AC-PIO-DESN model had higher prediction performance than the ESN, Leaky-ESN, and DESN models and better matched the actual characteristics of the four environmental parameters, providing an average MAPE of 8.0084%.
3. With the relative error of the daily dust prediction model between 0.65% and 54%, the proposed method can provide data support for cleaning operation and maintenance of PV field as well as grid connection scheduling.

Although the proposed method provided excellent results for predicting the dust accumulation on PV panels, the environmental variables and the dust types are highly variable in practical applications. In a future study, we will consider additional factors related to dust accumulation to improve the model's accuracy.

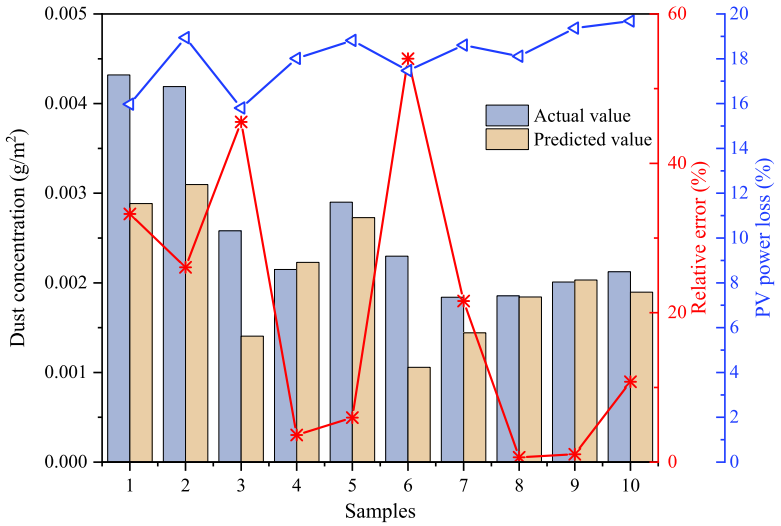

Fig. 11. Comparison of actual results and predicted results.

CRediT authorship contribution statement

Siyuan Fan: Conceptualization, Methodology, Writing – original draft. **Mingyue He:** Writing – review & editing. **Zhenhai Zhang:** Software, Validation.

Declaration of competing interest

The authors declare that they have no known competing financial interests or personal relationships that could have appeared to influence the work reported in this paper.

Data availability

No data was used for the research described in the article.

Acknowledgments

This work was supported by the Science and Technology Development Program of Jilin Province Grant. YDZJ202301ZYTS399, and the Doctoral Research Foundation Project of Northeast Electric Power University Grant. BSJXM-2022207.

References

[1] Y.N. Chanchangi, A. Ghosh, S. Sundaram, et al., Dust and PV performance in Nigeria: A review, Renew. Sustain. Energy Rev. 121 (2020) 109704.
[2] K. Yap, C. Sarimuthu, J. Lim, Artificial intelligence based MPPT techniques for solar power system: A review, J. Mod. Power Syst. Clean Energy 8 (2020) 1043–1059.
[3] Z. Wu, S. Yan, Z. Wang, et al., The effect of dust accumulation on the cleanliness factor of a parabolic trough solar concentrator, Renew. Energy 152 (2020) 529–539.
[4] B. Laarabi, Y.E. Baqqal, A. Dahrouch, et al., Deep analysis of soiling effect on glass transmittance of PV modules in seven sites in Morocco, Energy 213 (2020) 118811.
[5] M.A.T. Alnasser, A.M.J. Mahdy, K.I. Abass, et al., Impact of dust ingredient on photovoltaic performance: An experimental study, Sol. Energy 195 (2020) 651–659.
[6] Y.N. Chanchangi, A. Ghosh, S. Sundaram, et al., An analytical indoor experimental study on the effect of soiling on PV, focusing on dust properties and PV surface material, Sol. Energy 203 (2020) 46–68.
[7] W. Javed, B. Guo, B. Figgis, et al., Dust potency in the context of solar photovoltaic (PV) soiling loss, Sol. Energy 220 (2021) 1040–1052.
[8] S. Fan, W. Liang, G. Wang, et al., A novel water-free cleaning robot for dust removal from distributed photovoltaic (PV) in water-scarce areas, Sol. Energy 241 (2022) 553–563.
[9] S. Yan, S. Zhao, X. Ma, et al., Thermoelectric and exergy output performance of a Fresnel-based HCPV/T at different dust densities, Renew. Energy 159 (2020) 801–811.
[10] M.M.H. Mithhu, T.A. Rima, M.R. Khan, Global analysis of optimal cleaning cycle and profit of soiling affected solar panels, Appl. Energy 285 (2021) 116436.
[11] T. Zhu, H. Zhou, H. Wei, et al., Inter-hour direct normal irradiance forecast with multiple data types and time-series, J. Mod. Power Syst. Clean Energy 7 (2019) 1319–1327.
[12] H. Lu, B. He, W. Zhao, Experimental study on the super-hydrophobic coating performance for solar photovoltaic modules at different wind directions, Sol. Energy 249 (2023) 725–733.
[13] W. Yao, X. Kong, A. Xu, et al., New models for the influence of rainwater on the performance of photovoltaic modules under different rainfall conditions, Renew. Sustain. Energy Rev. 173 (2023) 113119.
[14] A. Salari, A. Hakkaki-Fard, A numerical study of dust deposition effects on photovoltaic modules and photovoltaic-thermal systems, Renew. Energy 135 (2019) 437–449.
[15] G. Aslan, K. Iman, E. Shahab, et al., Experimental investigation of dust deposition effects on photovoltaic output performance, Sol. Energy 159 (2018) 346–352.
[16] E. Klugmann-Radziemska, M. Rudnicka, Decrease in photovoltaic module efficiency because of the deposition of pollutants, J. Photovol. 10 (2020) 1772–1779.
[17] Y. Chen, Y. Liu, Z. Tian, et al., Experimental study on the effect of dust deposition on photovoltaic panels, Energy Procedia 158 (2019) 483–489.
[18] C. Shi, B. Yu, D. Liu, et al., Effect of high-velocity sand and dust on the performance of crystalline silicon photovoltaic modules, Sol. Energy 206 (2020) 390–395.
[19] H.A. Kazem, M.T. Chaichan, A.H.A. Al-Waeli, et al., A novel model and experimental validation of dust impact on grid-connected photovoltaic system performance in Northern Oman, Sol. Energy 206 (2020) 564–578.
[20] S. Sengupta, S. Sengupta, C.C. Chanda, et al., Comprehensive modeling of dust accumulation on PV modules through dry deposition processes, IEEE J. Photovolt. 10 (2020) 1148–1157.
[21] X. Yao, Y. Shao, S. Fan, et al., Echo state network with multiple delayed outputs for multiple delayed time series prediction, J. Franklin Inst. B 359 (2022) 11089–11107.
[22] L. Wang, Z. Su, J. Qiao, et al., A pseudo-inverse decomposition-based self-organizing modular echo state network for time series prediction, Appl. Soft Comput. 116 (2022) 108317.
[23] H. Wang, Y. Liu, P. Lu, et al., Echo state network with logistic mapping and bias dropout for time series prediction, Neurocomputing 489 (2022) 196–210.
[24] L. Sun, B. Jin, H. Yang, et al., Unsupervised EEG feature extraction based on echo state network, Inform. Sci. 475 (2019) 1–17.
[25] H. Wang, X. Long, X. Liu, fastESN: Fast echo state network, IEEE Trans. Neural Netw. Learn. Syst. (2022) 1–15.
[26] Z. Wu, S. Zeng, R. Jiang, et al., Explainable temporal dependence in multi-step wind power forecast via decomposition based chain echo state networks, Energy 270 (2023) 126906.
[27] Mustaqeem M. Ishaq, S. Kwon, A CNN-assisted deep echo state network using multiple time-scale dynamic learning reservoirs for generating short-term solar energy forecasting, Sustain. Energy Technol. Assess. 52 (2022) 102275.

[28] Y. Li, F. Li, Growing deep echo state network with supervised learning for time series prediction, Appl. Soft Comput. 128 (2022) 109454.
[29] P.K. Enaganti, A. Bhattacharjee, A. Ghosh, et al., Experimental investigations for dust build-up on low-iron glass exterior and its effects on the performance of solar PV systems, Energy 239 (2022) 122213.
[30] W. Huang, K. Zhou, K. Sun, et al., Effects of wind flow structure, particle flow and deposition pattern on photovoltaic energy harvest around a block, Appl. Energy 253 (2019) 113523.
[31] H. Jaeger, H. Hass, Harnessing nonlinearity: predicting chaotic systems and saving energy in wireless communication, Science 304 (2004) 78–80.
[32] S. Fan, X. Yao, S. Cao, et al., Temperature prediction of photovoltaic panels based on delayed echo state network, Acta Automat. Sinica 46 (2020) 2701–2710.
[33] H. Duan, P. Qiao, Pigeon-inspired optimization: A new swarm intelligence optimizer for air robot path planning, Int. J. Intell. Comput. Cybern. 7 (2014) 24–37.
[34] C. Hu, G. Qu, Y. Zhang, Pigeon-inspired fuzzy multi-objective task allocation of unmanned aerial vehicles for multi-target tracking, Appl. Soft Comput. 126 (2020) 109310.
[35] M. Coello, L. Boyle, Simple model for predicting time series soiling of photovoltaic panels, IEEE J. Photovolt. 9 (2019) 1382–1387.
[36] B.R. Paudyal, S.R. Shakya, Dust accumulation effects on efficiency of solar PV modules for off grid purpose: A case study of kathmandu, Sol. Energy 135 (2016) 103–110.
[37] B. Du, S. Huang, J. Guo, et al., Interval forecasting for urban water demand using PSO optimized KDE distribution and LSTM neural networks, Appl. Soft Comput. 122 (2022) 108875.
[38] P. Zhang, J. Wang, Z. Tian, et al., A genetic algorithm with jumping gene and heuristic operators for traveling salesman problem, Appl. Soft Comput. 127 (2022) 109339.
[39] S. Lun, H. Hu, X. Yao, The modified sufficient conditions for echo state property and parameter optimization of leaky integrator echo state network, Appl. Soft Comput. 77 (2019) 750–760.